Progress towards ignition on the National Ignition Facility

M. J. Edwards, P. K. Patel, J. D. Lindl, L. J. Atherton, S. H. Glenzer et al.

Citation: Phys. Plasmas **20**, 070501 (2013); doi: 10.1063/1.4816115
View online: http://dx.doi.org/10.1063/1.4816115
View Table of Contents: http://pop.aip.org/resource/1/PHPAEN/v20/i7
Published by the AIP Publishing LLC.

Progress towards ignition on the National Ignition Facility[a)]

M. J. Edwards,[1,b)] P. K. Patel,[1] J. D. Lindl,[1] L. J. Atherton,[1] S. H. Glenzer,[1] S. W. Haan,[1] J. D. Kilkenny,[2] O. L. Landen,[1] E. I. Moses,[1] A. Nikroo,[2] R. Petrasso,[3] T. C. Sangster,[4] P. T. Springer,[1] S. Batha,[5] R. Benedetti,[1] L. Bernstein,[1] R. Betti,[4] D. L. Bleuel,[1] T. R. Boehly,[4] D. K. Bradley,[1] J. A. Caggiano,[1] D. A. Callahan,[1] P. M. Celliers,[1] C. J. Cerjan,[1] K. C. Chen,[2] D. S. Clark,[1] G. W. Collins,[1] E. L. Dewald,[1] L. Divol,[1] S. Dixit,[1] T. Doeppner,[1] D. H. Edgell,[4] J. E. Fair,[1] M. Farrell,[2] R. J. Fortner,[1] J. Frenje,[3] M. G. Gatu Johnson,[3] E. Giraldez,[2] V. Yu. Glebov,[4] G. Grim,[5] B. A. Hammel,[1] A. V. Hamza,[1] D. R. Harding,[4] S. P. Hatchett,[1] N. Hein,[2] H. W. Herrmann,[5] D. Hicks,[1] D. E. Hinkel,[1] M. Hoppe,[2] W. W. Hsing,[1] N. Izumi,[1] B. Jacoby,[1] O. S. Jones,[1] D. Kalantar,[1] R. Kauffman,[1] J. L. Kline,[5] J. P. Knauer,[4] J. A. Koch,[1] B. J. Kozioziemski,[1] G. Kyrala,[5] K. N. LaFortune,[1] S. Le Pape,[1] R. J. Leeper,[6] R. Lerche,[1] T. Ma,[1] B. J. MacGowan,[1] A. J. MacKinnon,[1] A. Macphee,[1] E. R. Mapoles,[1] M. M. Marinak,[1] M. Mauldin,[2] P. W. McKenty,[4] M. Meezan,[1] P. A. Michel,[1] J. Milovich,[1] J. D. Moody,[1] M. Moran,[1] D. H. Munro,[1] C. L. Olson,[6] K. Opachich,[1] A. E. Pak,[1] T. Parham,[1] H.-S. Park,[1] J. E. Ralph,[1] S. P. Regan,[4] B. Remington,[1] H. Rinderknecht,[3] H. F. Robey,[1] M. Rosen,[1] S. Ross,[1] J. D. Salmonson,[1] J. Sater,[1] D. H. Schneider,[1] F. H. Séguin,[3] S. M. Sepke,[1] D. A. Shaughnessy,[1] V. A. Smalyuk,[1] B. K. Spears,[1] C. Stoeckl,[4] W. Stoeffl,[1] L. Suter,[1] C. A. Thomas,[1] R. Tommasini,[1] R. P. Town,[1] S. V. Weber,[1] P. J. Wegner,[1] K. Widman,[1] M. Wilke,[5] D. C. Wilson,[5] C. B. Yeamans,[1] and A. Zylstra[3]

[1]*Lawrence Livermore National Laboratory, P.O. Box 808, Livermore, California 94550, USA*
[2]*General Atomics, P.O. Box 85608, San Diego, California 92186, USA*
[3]*Plasma Fusion and Science Center, Massachusetts Institute of Science and Technology, 175 Albany Street, NW17, Cambridge, Massachusetts 02139, USA*
[4]*Laboratory for Laser Energetics, University of Rochester, 250 E. River Road, Rochester, New York 14623, USA*
[5]*Los Alamos National Laboratory, P.O. Box 1663, Los Alamos, New Mexico 87545, USA*
[6]*Sandia National Laboratory, P.O. Box 5800, Albuquerque, New Mexico 87185, USA*

(Received 26 March 2013; accepted 5 June 2013; published online 30 July 2013)

The National Ignition Facility (NIF) at Lawrence Livermore National Laboratory includes a precision laser system now capable of delivering 1.8 MJ at 500 TW of 0.35-μm light to a target. NIF has been operational since March 2009. A variety of experiments have been completed in support of NIF's mission areas: national security, fundamental science, and inertial fusion energy. NIF capabilities and infrastructure are in place to support its missions with nearly 60 X-ray, optical, and nuclear diagnostic systems. A primary goal of the National Ignition Campaign (NIC) on the NIF was to implode a low-Z capsule filled with ~0.2 mg of deuterium-tritium (DT) fuel via laser indirect-drive inertial confinement fusion and demonstrate fusion ignition and propagating thermonuclear burn with a net energy gain of ~5–10 (fusion yield/input laser energy). This requires assembling the DT fuel into a dense shell of ~1000 g/cm^3 with an areal density (ρR) of ~1.5 g/cm^2, surrounding a lower density hot spot with a temperature of ~10 keV and a ρR ~0.3 g/cm^2, or approximately an α-particle range. Achieving these conditions demand precise control of laser and target parameters to allow a low adiabat, high convergence implosion with low ablator fuel mix. We have demonstrated implosion and compressed fuel conditions at ~80–90% for most point design values independently, but not at the same time. The nuclear yield is a factor of ~3–10× below the simulated values and a similar factor below the alpha dominated regime. This paper will discuss the experimental trends, the possible causes of the degraded performance (the off-set from the simulations), and the plan to understand and resolve the underlying physics issues. © *2013 AIP Publishing LLC*. [http://dx.doi.org/10.1063/1.4816115]

I. INTRODUCTION

The National Ignition Facility (NIF) is the first laser system designed to demonstrate ignition and thermonuclear burn of deuterium-tritium-filled capsules. The NIF has been operational and conducting experiments since late in 2009.[1–11] A primary goal of the National Ignition Campaign (NIC) on the NIF was to demonstrate fusion ignition and burn via inertial confinement fusion (ICF). The NIC approach to ignition utilizes indirect drive, wherein the DT-filled capsule is placed inside a cylindrical cavity of a high-Z metal (a hohlraum), and the implosion drive (pressure) is provided by focusing laser energy onto the interior walls of

[a)]Paper MR1 1, Bull. Am. Phys. Soc. **57**, 200 (2012).
[b)]Invited speaker.

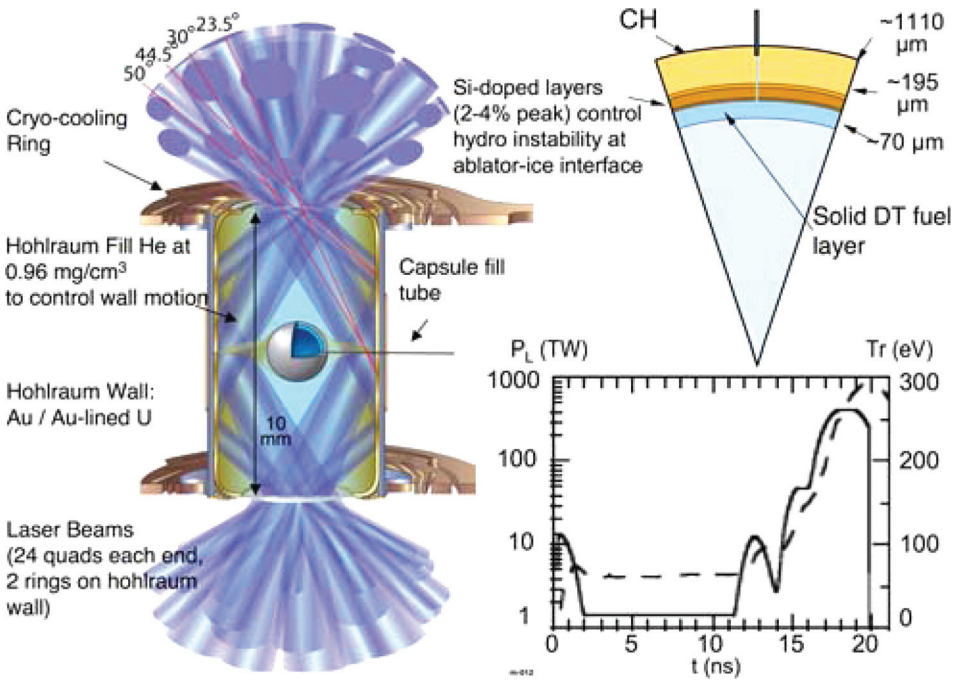

FIG. 1. Schematic of NIF ignition target and capsule and a typical laser pulse (solid line) and resulting simulated X-ray drive (dashed line) pulse. The hohlraum is made of uranium with a thin passivating layer of gold ~0.5 μm thick on the inside surface. It is filled with He gas at a density ~0.96 mg/cc, which controls wall motion for drive symmetry control. The dimensions have been selected based on recent NIF experiments to obtain symmetric implosions. The capsule ablator has five layers, three of which are doped with Si to control hydrodynamic instability at the ablator-ice interface. Heating of the inner clean CH layer by X-rays >1.8 keV, which pass through the ice, drives a Rayleigh-Taylor unstable configuration at the interface. The amount of Si is set to control the Atwood number such that instability growth is acceptable. The details of the design attempt to optimize the overall efficiency while controlling instability. (For a more complete description, see Ref. 6). The laser power is stepped in time to gradually increase the X-ray drive on the capsule such that the pressure in the ice is increased in four shocks from ~1 Mbar to a value in excess of 100 Mbar during the implosion phase. The steps are timed such that the shocks coalesce just inside the ice layer, which minimizes the entropy generation in the layer. The first shock enters the ice close to ~14 ns after it has traversed the ablator.

the hohlraum and converting it to X-rays (Figure 1). The temporal shape and the spatial profile and distribution of the input laser beams (and hence the X-ray drive) are tailored to assemble the D-T fuel into a dense shell of ~1000 g/cm^3, surrounding a lower density hot spot. Ignition is approached as the hot spot central temperature reaches a temperature of ~10 keV and a $\rho R \sim 0.3$ g/cm^2, approximately equivalent to an α-particle stopping range. Ignition will occur if the total ρR of the imploded fuel is $> \sim 1.5$ g/cm^2, so that the hot spot is confined long enough for the temperature to bootstrap by α-heating to several tens of keV. Achieving these ρR and T conditions require a low adiabat (low entropy), high convergence ~30–40 spherical implosion. This demands precise control over the laser pulse and target, which have been carefully designed to balance key implosion parameters of velocity (v), adiabat (a), hot spot shape (s), and ablator fuel mix (m).

Experiments are ongoing to study these four major control variables and have demonstrated that with the techniques developed (diagnostics, laser and target configuration options) we can observe, modify, and within certain constraints, control these variables. Cryogenic layering of the DT fuel with the DT-layer quality predicted to be required for ignition has been demonstrated. Symmetric implosions (P2 coefficient of X-ray emission > 10 keV from the DT hot spot ~6%) at peak hohlraum temperatures (T_r) of 300 eV have been achieved with laser energies in the range of 1.3- to 1.8-MJ and peak power of 450–500 TW with good absorption (85–90%) and low fast-electron preheat. Final fuel ρr at about 85% of the ignition point design has been obtained, and in separate experiments implosion velocities (v_{imp}) of 90% of that required for ignition. As shown in Table I, we have achieved a large fraction of the point design conditions in key areas independently, but not all at the same time. In addition, the hot spot pressures are approximately 2–3× below predictions, and mix is observed at lower velocities than predicted.

TABLE I. Key performance parameters from the NIC. Requirements for ignition point design are compared with the best values obtained from any experiment, and two experiments that both obtained an ITFX of ~0.1 with, respectively, the single highest neutron yield and single highest ρR.

	Ignition point design	Best in any experiment	Best coast in Figure 2 N111215	Best no coast in Figure 2 N120321
T_r (eV)	305	320	292	303
V_{imp} (km/s)	370	352	312	310
Convergence	36	48	32	44
Hot spot asymmetry	<10% P2	6% P2	24%P2	6% P2
Hot spot P (G Bar)	375	197	103	156
Main fuel ρr (g/cm^2)	1.5	1.33	0.90	1.31
T_{ion} (keV)	3.5	4.3	3.6	3.1
No burn DT equivalent yield (13–15 MeV)	3.5×10^{15}	7.5×10^{14}	7.5×10^{14}	4.2×10^{14}
Total DT yield	3.4×10^{17}	8.5×10^{14}	8.5×10^{14}	5.0×10^{14}
Mix mass (ng)	<100	0–150	120	287
Normalized ITFX	1.20	0.097	0.073	0.097

One metric for expressing progress toward ignition is the Experimental Ignition Threshold Factor (ITFX). The ITFX depends upon the experimentally measured neutron yield and the ratio of down-scattered neutrons (dsr) to unscattered neutrons, in a no alpha deposition implosion

$$ITFX = \left(\frac{Y_{13-15\,\mathrm{MeV}}}{3e15}\right)\left(\frac{dsr}{0.073}\right)^{2.3}. \quad (1)$$

$Y_{13\text{-}15\,\mathrm{MeV}}$ is the measured unscattered yield in the primary peak between 13 and 15 MeV. It is typically ~80% of the total DT primary yield which also includes downscattered neutrons. The dsr is approximately proportional to the areal density of the DT fuel ($\rho r \sim 21\ \mathrm{g/cm^2} \times \mathrm{dsr}\ \%$[12]). ITFX is related to the generalized Lawson criterion and is normalized so that an ITFX of 1 is defined as the condition in which the probability of a yield greater than 1 MJ on a given shot is 50%. Progress toward ignition can be graphically represented as shown in Figure 2 in which cryo-layered target neutron yield is plotted versus the dsr, where the contours drawn represent constant ITFX.

The yields plotted in this figure arise primarily from compressional heating of the hot spot during the implosion process. As the implosion quality approaches that required for ignition the enhancement due to alpha heating becomes significant. Within the context of ITFX, this yield provides a metric for the underlying quality of the implosion needed to get into a regime in which the alpha particle deposition becomes significant. In these experiments, alpha heating is estimated to be no more than a 20% effect on yield. The ignition regime is above ITFX of 1, while the alpha-dominated regime, in which the yield enhancement from alpha particle deposition exceeds the yield from compression alone, occurs for an ITFX of ~0.3–0.5. The progress in ITFX shown in Figure 2 can be summarized as follows:

- The improvement in ITFX from the first cryogenic layered implosion in September 2010 to values of 0.02 in early 2011 (the green squares in Figure 2), mostly in the neutron yield, was achieved by increasing the laser power.
- During 2011, ITFX was increased to ~0.08 (the blue squares). This was achieved with improved shock timing as well as by increasing implosion velocity using Si-doped rather than Ge-doped CH ablators, increasing laser performance and improving implosion symmetry. In the majority of experiments, the laser pulse was turned off when the ablator/fuel interface was at ~600 μm radius, and hence the term "coast" signifies that during the final implosion stage, the DT fuel was "coasting" and decompressing. The variation in yield during this phase is attributed primarily to deliberate variation in laser power, energy, and the resulting variation in implosion velocity as well as deliberate changes in hot spot shape. The variation in dsr can be attributed to shot-to-shot shock timing variations due to laser pulse variations.
- In 2012, the slope of the rise of the fourth pulse (see Figure 1) was decreased, producing an implosion with higher compression and lower adiabat. The length of the fourth pulse was also extended to better maintain compression of the shell during final convergence, producing a higher dsr, or ρr, resulting in an improved ITFX of ~0.1, although at a lower velocity (the purple square "No Coast" points in Figure 2). We attribute the variation in yield during this phase to shot-to-shot variations in mix (more compression leads to thinner shells in-flight, which are more susceptible to mix). The variation in dsr is strongly correlated with shot-to-shot differences in the merge depth of the first 2 shocks[3] due to laser pulse variations.

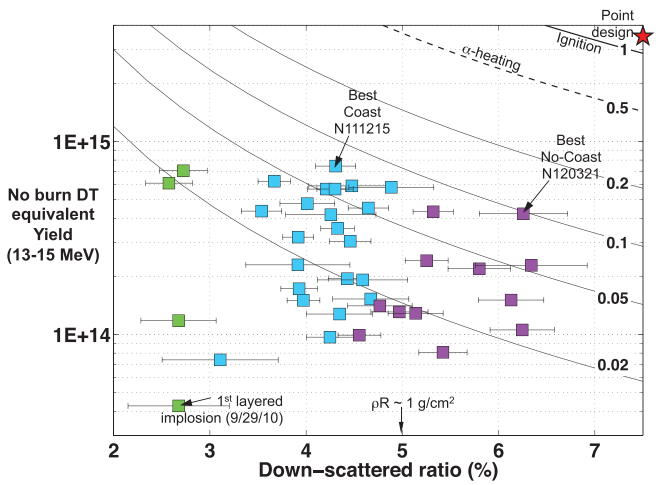

FIG. 2. DT equivalent yield (13–15 MeV) vs. down-scattered ratio for all cryogenic layered implosions on the NIF. Shots are grouped by pre shock-timing (green squares), "Coast" drives (blue squares), and "Extended Pulse-No Coast" drives (purple squares). Lines represent constant ITFX. The experiments that had the single highest neutron yield (N111215) and single highest ρR (N120321), respectively, are indicated.

Table I and Figure 2 show that the integrated implosion performance is currently limited to an ITFX of ~0.1 and emphasize (as was mentioned above) that we have achieved key implosion parameters (yield, temperature, velocity, ρR) close to the ignition point design in separate, independent experiments, but not at the same time. It appears that in the best performing experiments, we are essentially "trading" neutron yield for ρR.

As will be discussed in more detail in Secs. II–V, the experimental trends can be reproduced by simulation, but are offset (e.g., yield vs. ion temperature or hot spot pressure vs. implosion velocity). The estimated mix in the hot spot provides the strongest correlation for the degraded performance (discussed further in Sec. III), but there is no single parameter (e.g., higher Rayleigh Taylor growth of the ablator fuel interface) or observable that can explain the discrepancies. Angular measurements of down-scattered neutrons indicate that there could be low spatial mode asymmetries in the compressed main fuel, which may explain some of the deficit in pressure and the larger than expected mix.

At this time, the theoretical and experimental efforts are being focused on measuring and quantifying the deviation (degradation) from expected (modeled) performance. Experiments include campaigns to measure and provide improved, quantitative modeling of the hohlraum, and the resulting time-dependent X-ray drive, as well as capsule implosion and mix. These efforts will also be discussed in Secs. III–V.

II. DT CAMPAIGN

The cryogenic layered campaign has included 38 shots with tritium-hydrogen-deuterium (THD) fuel layers. Of these, 28 shots have used a 50:50 DT fuel mixture. As the campaign has progressed, a range of laser pulse shapes have been employed and hohlraum and capsule designs fielded (Figure 3). Peak power ranged from 290 to 450 TW, the fourth pulse peak rate of rise from 170 TW/ns to 500 TW/ns, the hohlraum size from 10.0 mm long by 5.44 mm in diameter to 9.4 mm-long by 5.75 mm in diameter, both Au and 0.6 μm Au-lined U walls, Ge and Si dopants in the CH ablator with peak concentrations of 1, 2, and 4% by atomic fraction, and ablator thicknesses between 189 and 217 μm. The peak fuel velocity has ranged from 290 to 350 km/s. The measured primary DT yield, between 13 and 15 MeV, has varied between 7.5×10^{13} and 7.5×10^{14} neutrons, and the burn-averaged ion temperature between 1.8 and 4.2 keV. The principal source of this variability appears to be mix of CH ablator into the hot spot.

III. HOT SPOT MIX

Mix of CH ablator into the hot spot will increase radiation loss, cool the hot spot, and reduce the neutron yield. Provided the shell remains relatively intact, the stagnation pressure is not much affected and any cooling results in higher density. A model has been developed that uses the absolute measured X-ray emission and primary neutron yield to estimate the level of CH mix into the hot spot.[13] In a 1D uniform hot spot model, the total primary neutron yield is given by

$$Y_{DT} \approx f_D f_T \frac{A_v^2}{\bar{A}^2} \rho_{DT}^2 \sigma_{DT} v(T_i) V \Delta t, \tag{2}$$

where f_D and f_T are the atomic fractions of deuterium and tritium ions, respectively; $\bar{A}$ is the mean atomic mass; A_v is Avogadros number; ρ_{DT} is the density; $\sigma_{DT}v(T_i)$ is the DT reactivity cross-section at the ion temperature T_i; V is the hot spot volume; and Δt the burn duration. The total X-ray emission from the hot spot, after attenuation by the cold fuel and ablator shell, can be written as

$$X_\nu = 4\pi \int j_{DT}.dVdt \times (1 + \Sigma x_i Z_i) \times \left(1 + \Sigma x_i \frac{j_i}{j_{DT}}\right) \times e^{-\tau_\nu^{\text{shell}}}, \tag{3}$$

where j_{DT} is the frequency-dependent emissivity of DT; the term $(1 + \Sigma x_i Z_i)\left(1 + \Sigma x_i \frac{j_i}{j_{DT}}\right)$ represents the enhancement due to mix of ions with atomic number Z_i, emissivity j_i, and fraction x_i of the total number of D and T atoms; and τ_ν^{shell} is the optical depth of the shell.

The emission coefficients are obtained from fits to Detailed Configuration Accounting (DCA) model calculations[14] and have the form

$$j_{DT} \cong \frac{2.2}{\bar{A}^2} \rho_{DT}^2 \frac{1 - e^{-h\nu/kT_e}}{(h\nu)^{3.33}} B_\nu(T_e), \tag{4}$$

where $B_\nu(T_e)$ is the Planck function and $h\nu$ is the photon energy in units of keV. For a DT plasma, the emitted radiation is predominantly free-free emission, but for CH both free-free and free-bound contributions are important. The ratio of the X-ray to neutron yield is then independent of the hot spot density, volume, and burnwidth, and scales only with temperature, shell attenuation, and mix fraction

$$\frac{X_\nu}{Y_{DT}} = 4\pi \frac{2.2}{f_D f_T A_v^2} \frac{B_\nu(T_e)}{\langle \sigma_{DT} v(T_i) \rangle} \frac{1 - e^{-h\nu k/T_e}}{(h\nu)^{3.33}} \times (1 + \Sigma x_i Z_i) \times \left(1 + \Sigma x_i \frac{j_i}{j_{DT}}\right) \times e^{-\tau_\nu^{shell}}. \tag{5}$$

The neutron yield and ion temperature are measured by a suite of nuclear diagnostics.[15–17] The X-ray emission from the hot spot is measured by two absolutely calibrated diagnostics, the Ross Pair diagnostic,[18,19] which spatially images the hot spot in five broad energy bands above 6 keV, and the South Pole Bang Time diagnostic,[20,21] which records the temporally resolved emission in a narrow band at 10.85 ± 0.3 keV. Assuming $T_e = T_i$, Eqs. (2) and (5) can then be used to calculate the optical depth of the shell, and the atomic fraction and mass of CH present in the hot spot. To compensate for uncertainties in absolute detector response, the X-ray to neutron yield ratio is normalized to the cleanest shot, which is taken to have a nominal mix mass of ~30 ng. Changing this value up or down would result in a corresponding scaling in the mix mass inferred for the other shots. While this model assumes the CH to be uniformly distributed within the hot spot volume; it is also a good approximation in the event of the CH being localized in small regions within the hot spot. This is because the x-ray

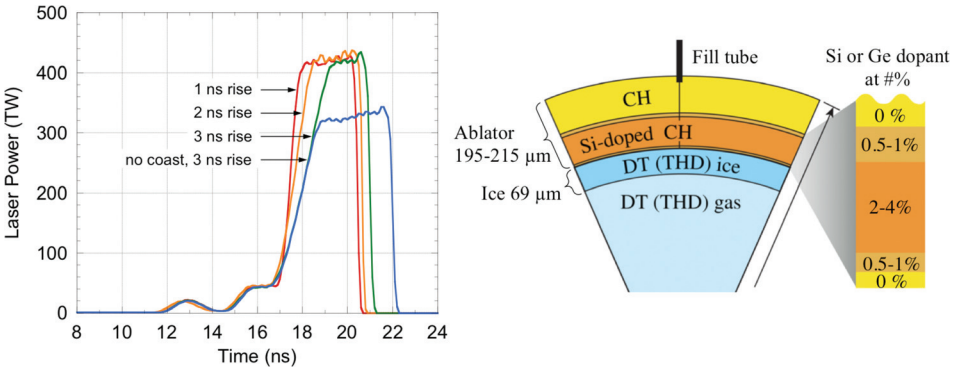

FIG. 3. Pulse shape changes have included variations in the peak power, the 4th pulse rise time, and "no coast" drives with extended pulses, as well as smaller tuning adjustments to the picket, trough, and 2nd and 3rd shocks based on keyhole shock timing measurements. The capsule dopant was changed from Ge to Si to improve radiation coupling, and the dopant concentration varied to control the fuel-ablator Atwood number.

emission from the CH is linearly proportional to the ion density and electron density. For small mix fractions, the electrons predominantly come from the DT and their density is approximately constant. Hence, the total or volume-integrated x-ray emission is dependent only on the total number of CH ions and not on their distribution within the hot spot.

A large variation in CH mix mass is observed across the DT campaign, with values ranging up to 3000–4000 ng. The peak fuel velocity for the bulk of these shots is between 300 and 340 km/s, where simulations do not predict significant ablator mix into the hot spot, other than ~30 ng due to the fill tube. The observed level of mix does not correlate strongly with any single laser drive or target parameter, including the peak laser power. Shots with extended drives, designed to maintain late time compression of the shell, do exhibit a slightly greater propensity for mix, though they also have higher levels of Si dopant in the ablator which is predicted to increase ablation front instability growth. The measured neutron yield is quite strongly correlated with the observed mix (Figure 4). A steep drop in neutron yield is associated with ablator mix mass >100–200 ng. This correlation suggests that ablator mix into the hot spot plays a dominant role in explaining the observed variability in yield.

Figure 5(a) plots the measured neutron yield vs. ion temperature for all the DT shots to date. The data follow a power law scaling of the form $Y_{DT} \sim T_i^k$, but with an exponent smaller than the $k \cong 4.7$ expected from the theoretical scaling for 1D neutron yield in the absence of alpha heating.[22] This slower scaling is consistent with assuming DT pressure $\sim nT_i$ is conserved for small amounts of mix, such that $Y_{DT} \sim n^2T_i^{4.7}$ is then $\sim T^{2.7}$. The data are also offset from simulations. Two-dimensional post shot simulations were performed for a number of the shots shown. The simulations, described in detail in Clark *et al.*,[23] incorporate our best knowledge of the delivered laser pulse shape and capsule and ice surfaces, as measured for each shot. A 2D integrated hohlraum calculation provides the radiation drive spectrum for a highly resolved 2D capsule-only simulation. The drive is adjusted in 1D to match shock-timing measurements of

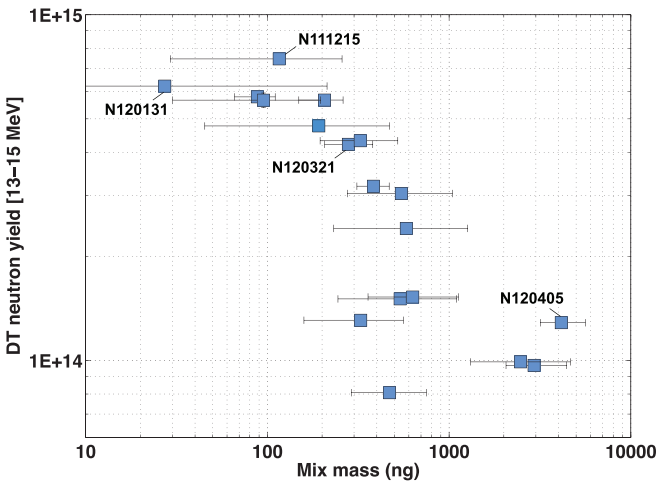

FIG. 4. Measured DT neutron yield vs. inferred CH mix mass in hot spot of 50:50 DT layered implosions. The mix mass is normalized to shot N120131 which is assumed to have a nominal mix mass of ~30 ng. The labels are the last four digits of the shot number.

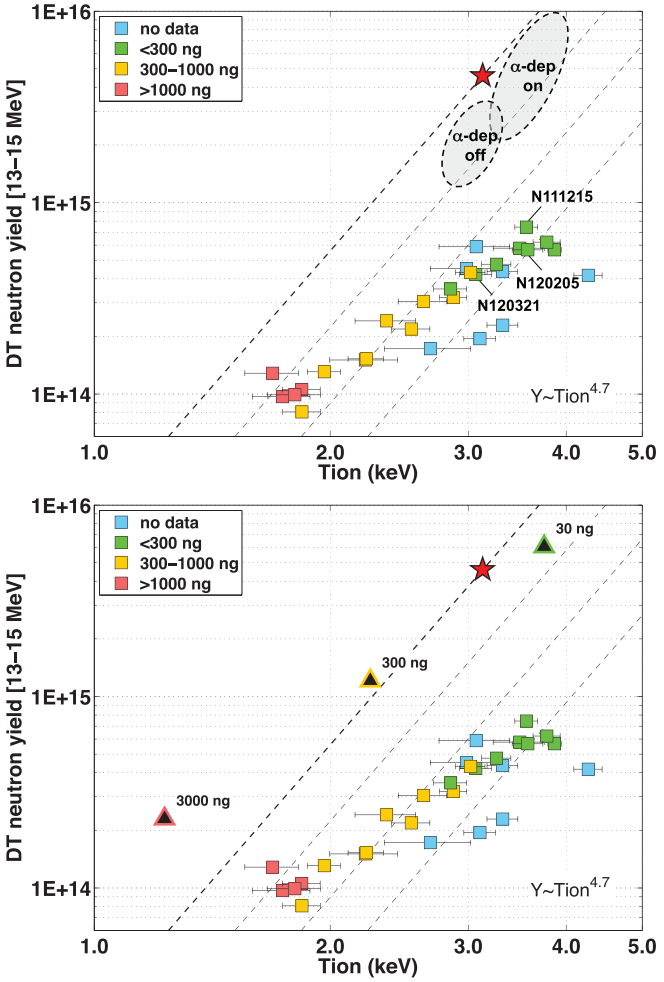

FIG. 5. (A) Neutron yield vs. ion temperature of 50:50 DT layered implosions. Shots are shown by level of CH mix into hot spot. Dotted lines are theoretical 1D scaling curves at different values of ρR.[21] The star represents the no-burn equivalent (alpha deposition off) of a simulation giving 1 MJ yield. Oval regions (top) encompass sets of 2D post shot capsule simulations with and without alpha deposition. (B) Triangles mark simulations of shot N120321 with 30, 300, and 3000 ng of CH preloaded into the DT gas.

the first three shocks from equivalent keyhole targets,[24] and to match in-flight measurements of the shell trajectory from convergent ablation targets.[25,26] The fourth pulse is adjusted to match the measured capsule trajectory, neutron bang time and dsr. The choice to approximately match the measured dsr assumes that 3D effects are relatively small, which may not be the case in practice as we discuss later. Simulations were performed both with alpha deposition on and off, and the results for all shots simulated to date fall within the two relatively small regions marked in grey in Figure 5(a). The experimental yields are 3-20× lower than predicted, ranging from the cleanest to most mixed shots. The different dashed lines in the figure correspond to different hot spot densities for a given hot spot mass, with density increasing toward the upper left corner and decreasing toward the lower right. The simulations predict higher hot spot density than observed experimentally. The slope of the experimental data is therefore consistent with the hot spot becoming smaller and denser with increasing mix. It is difficult to replicate the observed levels of mix in the simulations, but we can approximate the effect by preloading the DT gas in the capsule

with a given amount of CH. This method is used to incorporate the effect of the ~30 ng of CH mix expected from the fill tube. Figure 5(b) shows the results of increasing this preloaded mix to 300 and 3000 ng of CH in simulations with alpha deposition on. The yield and ion temperature drop precipitously, with a slope similar to the experimental slope. This supports the hypothesis that hot spot mix is primarily responsible for the observed trend in the data. There remains, however, a significant offset in yield between simulation and data, indicating the presence of other unaccounted for factors.

IV. HOT SPOT MODEL AND PRESSURE-VELOCITY

Insight into the implosion process can be gained by considering the pressure of the fuel at stagnation. The Rev 5-point design requires a burn-weighted hot spot pressure of 375 Gbar to be attained in a no alpha deposition implosion.[1] The pressure can be calculated from the ion temperature and the DT density derived from Eq. (2), using the hot spot volume measured from equator and polar self-emission X-ray imaging and burn duration measured from gated X-ray imaging and the gamma reaction history (GRH) diagnostics.[27] A correction is made to include the contribution of CH mix to the total pressure. Figure 6 plots the hot spot pressure against peak fuel velocity, with the shots separated by coast and no-coast drives. The two groups of shots broadly scale with the expected velocity^3 dependence. The v^3 dependence can be understood as follows. The pressure at stagnation will scale approximately as $\rho_{if}v^2$ where ρ_{if} is the in-flight density of the DT fuel and v its velocity. For given adiabat, α, the fuel pressure in-flight is given by $P_{if} \sim \alpha\rho_{if}^{5/3}$ or $\rho_{if} \sim (P_{if}/\alpha)^{3/5}$. The implosion velocity scales approximately as gt, where g is the shell acceleration and t is the time over which the acceleration occurs. The acceleration scales as $g \sim 4\pi R^2 P_{if}/M$, where M is the mass of the shell, and the time t is set by $R \sim 1/2\ gt^2$ where R is ~ the capsule radius. Thus, the implosion velocity scales as $v \sim g^{1/2} \sim P_{if}^{1/2}$ or $P_{if} \sim v^2$. Hence, $\rho_{if} \sim v^{6/5}$ and $\rho_{if}v^2 \sim v^3$. If the ablation pressure is not maintained until the capsule is committed to stagnation without experiencing decompression from rarefaction waves, an additional factor must be introduced to account for this. This explains the difference between the two classes of shots described in Figure 6.

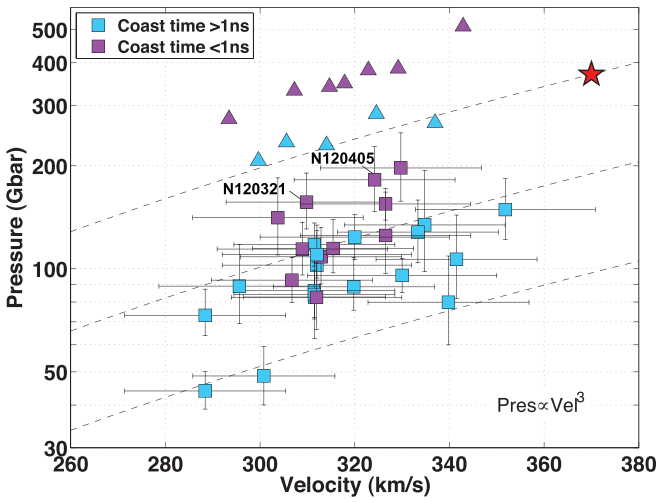

FIG. 6. Inferred pressure at stagnation vs. peak fuel velocity. Experiments [squares] and post shot simulations [triangles] are grouped by coasting (coast time >1 ns) and no coasting (coast time <1 ns) drives. The star is the point design value with alpha deposition turned off. Dotted lines represent the theoretical scaling with velocity along the ignition trajectory (top line) and fractions thereof.

The pressures achieved in the coast shots are 2-4 times lower than predicted by both theory and simulations. The simulations in this case are 2D integrated hohlraum simulations using "symmetrized" drives that give effectively near-1D performance.[28] The pressure offset of the coast series shows that a factor of two pressure deficiency would still be expected if driven at the point design velocity of 370 km/s. The no coast drive results in higher stagnation pressure, reducing the offset to the ignition scaling curve, though not eliminating it. However, another factor must be considered. While shot N120321, with a peak velocity of 310 km/s, achieves reasonably high yield with relatively low mix, shots driven with higher peak power attaining velocities of 325–330 km/s (e.g., N120405) exhibit heavy ablator mix and a large drop in yield, despite their pressure following the expected scaling. This highlights the fact that even after the pressure gap is closed in the current operating space, scaling to the point design velocity may involve contending with the increasing effects of hydrodynamic instabilities. It is also possible, however, that low mode asymmetries (see Sec. V) are amplifying the effects of higher mode instability. This will only be unraveled by further dedicated experiments.

V. ENERGY PARTITION OF FUEL

ICF implosions rely on the efficient conversion of shell kinetic energy to hot spot internal energy to produce the necessary conditions for alpha heating. The chart in Figure 7 examines the partition of energy in the fuel for one of the better performing shots, N120205, which achieved a total DT yield of 6.4×10^{14} neutrons and an ion temperature of 3.6 keV. Post shot simulations of this target have been performed in one, two, and three dimensions.[23] The 2D

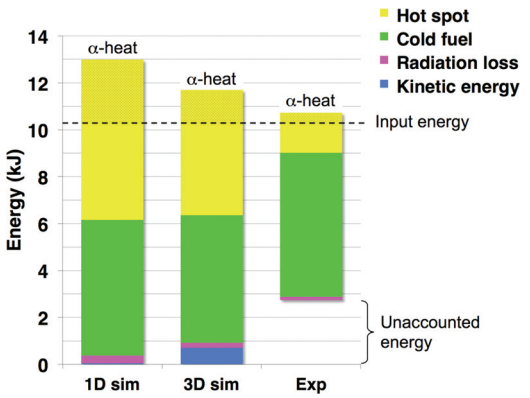

FIG. 7. Energy partition of DT fuel at stagnation (Shot N120205), from 1D and 3D capsule-only simulations, and inferred from experiment using a 3D static thermodynamic model. Plotted are the internal energy of the fuel forming the hot spot and cold fuel, radiation loss from the fuel, and kinetic energy of the fuel. The dotted horizontal line represents the "input energy" available to the fuel, estimated from the kinetic energy of the shell at peak velocity and additional PdV work done on the fuel during deceleration.

simulations resolve up to mode 1000, but in this 3D case, the resolution is limited to mode 50. The peak fuel implosion velocity was 299 km/s, corresponding to a kinetic energy of 7.6 kJ. Another 0.5 kJ is in the form of internal energy at this time. From the time of peak velocity to stagnation, the simulations predict that an additional 2.2 kJ of PdV work is done by the ablator on the fuel, giving a total of 10.3 kJ of energy delivered to the fuel at stagnation. In 1D, there is an almost complete conversion of kinetic energy to internal energy in the fuel, with the hot spot containing 6.8 kJ, of which 2.5 kJ is from alpha heating. Most radiation from the hot spot is reabsorbed in the cold fuel. In 3D, this efficiency is reduced because of non-radial mass flow arising from local non-uniformities or perturbations in the incoming shell. In this case, the hot spot internal energy is reduced to 5.4 kJ, of which 1.5 kJ is from alpha heating, and 0.7 kJ remains as unconverted kinetic energy in the fuel. A 3D static thermodynamic model of the fuel has been developed that uses both X-ray and nuclear diagnostic information to constrain the properties of the hot spot and cold fuel.[29] The hot spot density, pressure, and volume are determined in a similar manner to the 1D model described earlier, but extended to 3D dimensions in (r, θ, ϕ) space. The hot spot is surrounded by a cold DT shell approximated by a Gaussian radial distribution that is constrained by the initial DT fuel mass and down-scattered neutron measurements along a number of lines of sight. For N120205, the model estimates the hot spot internal energy to be 1.7 kJ, of which 0.4 kJ is from alpha heating. In this model, the hot spot ρR is estimated to be $\sim$ 0.1 g/cm^2, which is roughly twice the alpha stopping range at these temperatures. The internal energy of the cold fuel is estimated at 6.1 $\pm$ 1.3 kJ. It has a large uncertainty due to the difficulty of constraining the cold fuel volume in the absence of direct radiographic measurements. As seen in Figure 7, this leaves approximately 2.7 $\pm$ 1.3 kJ of energy unaccounted for, presumably in unconverted kinetic energy of the fuel or in "hot spot" that did not form properly and remained cold.

One hypothesis that may account for this discrepancy is the presence of large odd or even mode asymmetries. In simulations, these can have the effect of pinching off regions of the hot spot, preventing them from becoming hot. Evidence of an asymmetric cold fuel distribution has emerged from several nuclear diagnostic measurements. Neutron time-of-flight measurements of the dsr have shown persistent differences of $\sim$20% along different lines of sight. Unscattered primary neutron measurements made with flange nuclear activation detectors (FNADS) mounted at seventeen locations around the target chamber have revealed yield variations in some shots that correspond to factors of 2-3$\times$ differences in line-of-sight ρR[16] although it has not been possible to relate these variations to any systematic low mode fuel shape asymmetry. The yield distribution for an example shot is shown in Figure 8. Additionally, recent 2D X-ray radiographic measurements of Symcap targets

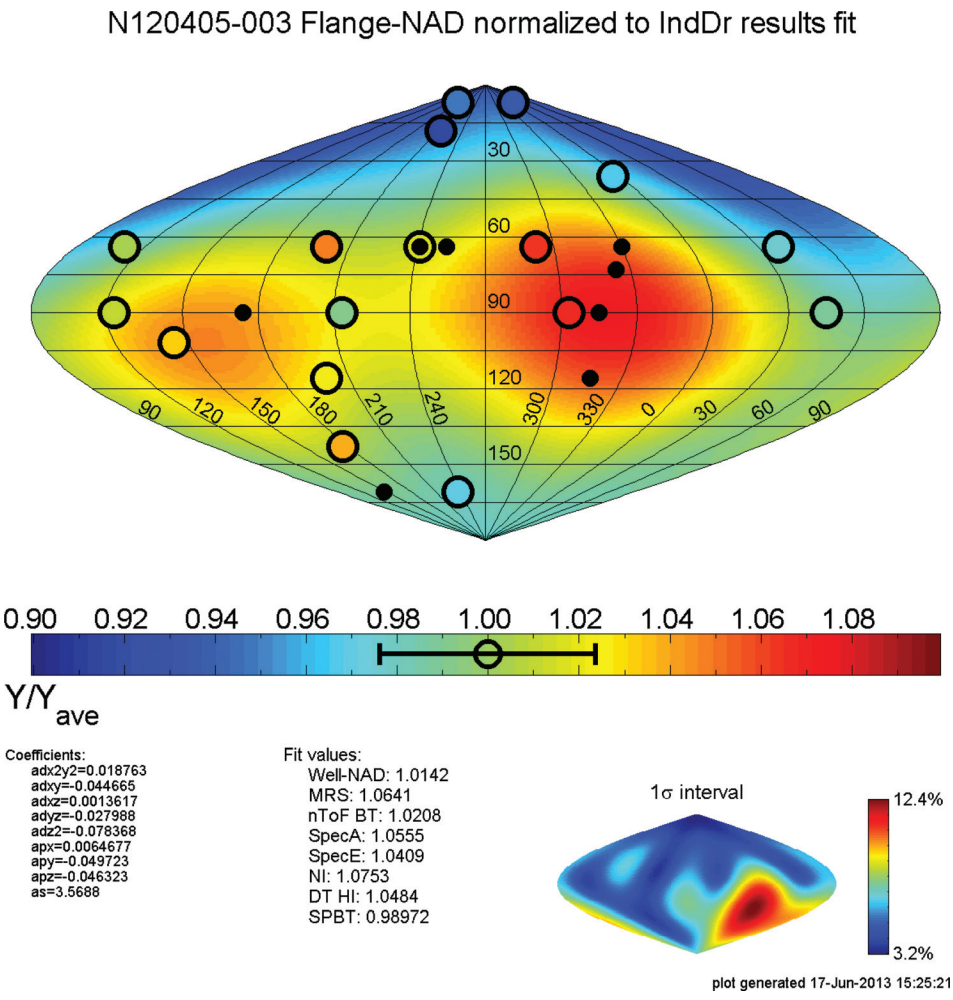

FIG. 8. Normalized yield (open circles) measured by FNADS at 17 locations around target chamber. Background color is a fit of the data to a low-order spherical harmonic distribution. Note that depending on the composition of the modes included in the harmonic distribution, different fits may be obtained.

(DHe^3-filled warm capsules) have shown significant P2 and P4 asymmetries of the shell in-flight.

VI. SUMMARY AND FUTURE DIRECTIONS

During the NIC, the demanding requirements set by the ignition point design for targets, diagnostics, and the laser were largely met, and experiments were developed using surrogate targets to measure and manipulate the key attributes of an ignition implosion. As a result, significant progress has been made toward forming the DT fuel conditions necessary for ignition. In particular, fuel areal densities of 1.3 g/cm^2 or 85% of the point design value have been achieved, and hot spot temperatures in many implosions are comparable to those predicted to be needed for strong alpha heating. However, the highest neutron yield obtained has been 8.5×10^{14}, resulting in a hot spot heating rate a factor of $\sim 10\times$ below that for which alpha deposition would begin to cause bootstrap heating leading to ignition. The neutron yields are also a similar factor below detailed post shot 2D and 3D implosion simulations that included the best knowledge of shock timing, implosion trajectory, and capsule surfaces. In these simulations, the implosions were relatively spherical and the impact of hydrodynamic instabilities was small, leading to little reduction of the hot spot clean volume and very little mixing of ablator material into the hot spot. In the best performing implosions in which there was little mix of ablator into the hot spot (low mix experiments), data analysis indicates that the hot spot density was ~ 2–$3\times$ below these post shot simulations while the temperatures were comparable. This suggests that the lower hot spot density may be largely responsible for the disagreement between simulation and experiment in these cases. A leading hypothesis for this discrepancy is that low mode X-ray drive asymmetries are larger than predicted by the hohlraum simulations used to construct the time-dependent drive symmetry for the detailed post shot implosion simulations. Nuclear activation data and recent 2D radiographic measurements indicate significant implosion asymmetries not included in the post shot implosion simulations. Including significant X-ray drive asymmetry in these simulations leads to implosions that can exhibit many of the characteristics of these experiments, but the details of the asymmetries remain to be quantified and understood. Experiments to do this and subsequently reduce the asymmetries to acceptable levels are currently under way.

Since the hot spot temperatures in these low mix experiments are comparable to those predicted by simulations, the lower hot spot densities also translate to lower pressures than simulated. The peak stagnation pressure achieved was ~ 150 Gbar compared with 375 Gbar for the point design. Some implosions reached higher pressures ~ 200 Gbar but also exhibited significant mix of ablator material into the hot spot, which resulted in significant radiative cooling and low neutron yields. The neutron yields observed in all the cryogenic DT implosion experiments correlated strongly with the amount of ablator mixed into the hot spot. This has not been predicted by the post shot simulations, which leave the central fuel relatively clean. However, post shot simulations in which ablator material is artificially mixed into the central gas approximately reproduce the trend seen in the data, although the yields, pressures, and densities remain offset and higher than the experiments. Future experiments will measure the ablation front instability growth directly from known initial perturbations, and implosions with higher adiabat than the point design are being developed. These implosions are predicted to have substantially less ablation front growth than the point design and should help isolate the source of ablator mixing into the hot spot.

In addition to these studies of 3D hydrodynamics effects, experiments are planned to better understand laser plasma interactions in the hohlraum, and we continue to advance experimental techniques and diagnostics (optical, X-ray and nuclear) to continue to increase our knowledge of the implosions.

[1]M. J. Edwards, J. D. Lindl, B. K. Spears, S. V. Weber, L. J. Atherton, D. L. Bleuel, D. K. Bradley, D. A. Callahan, C. J. Cerjan, D. Clark, G. W. Collins, J. E. Fair, R. J. Fortner, S. H. Glenzer, S. W. Haan, B. A. Hammel, A. V. Hamza, S. P. Hatchett, N. Izumi, B. Jacoby, O. S. Jones, J. A. Koch, B. J. Kozioziemski, O. L. Landen, R. Lerche, B. J. MacGowan, A. J. MacKinnon, E. R. Mapoles, M. M. Marinak, M. Moran, E. I. Moses, D. H. Munro, D. H. Schneider, S. M. Sepke, D. A. Shaughnessy, P. T. Springer, R. Tommasini, L. Bernstein, W. Stoeffl, R. Betti, T. R. Boehly, T. C. Sangster, V. Yu. Glebov, P. W. McKenty, S. P. Regan, D. H. Edgell, J. P. Knauer, C. Stoeckl, D. R. Harding, S. Batha, G. Grim, H. W. Herrmann, G. Kyrala, M. Wilke, D. C. Wilson, J. Frenje, R. Petrasso, K. Moreno, H. Huang, K. C. Chen, E. Giraldez, J. D. Kilkenny, M. Mauldin, N. Hein, M. Hoppe, A. Nikroo, and R. J. Leeper, Phys. Plasmas **18**, 051003 (2011).

[2]S. H. Glenzer, B. K. Spears, M. J. Edwards, E. T. Alger, R. L. Berger, D. L. Bleuel, D. K. Bradley, J. A. Caggiano, D. A. Callahan, C. Castro, D. T. Casey, C. Choate, D. S. Clark, C. J. Cerjan, G. W. Collins, E. L. Dewald, J. G. Di Nicola, P. Di Nicola, L. Divol, S. N. Dixit, T. Doppner, R. Dylla-Spears, E. G. Dzenitis, J. E. Fair, L. J. A. Frenje, M. Gatu-Johnson, E. Giraldez, V. Glebov, S. M. Glenn, S. W. Haan, B. A. Hammel, S. P. Hatchett II, C. A. Haynam, R. F. Heeter, G. M. Heestand, H. W. Herrmann, D. G. Hicks, D. M. Holunga, J. B. Horner, H. Huang, N. Izumi, O. S. Jones, D. H. Kalantar, J. D. Kilkenny, R. K. Kirkwood, J. L. Kline, J. P. Knauer, B. Kozioziemski, A. L. Kritcher, J. J. Kroll, G. A. Kyrala, K. N. LaFortune, O. L. Landen, D. W. Larson, R. J. Leeper, S. Le Pape, J. D. Lindl, T. Ma, A. J. Mackinnon, A. G. MacPhee, E. Mapoles, P. W. McKenty, N. B. Meezan, P. Michel, J. L. Milovich, J. D. Moody, A. S. Moore, M. Moran, K. A. Moreno, D. H. Munro, B. R. Nathan, A. Nikroo, R. E. Olson, C. D. Orth, A. Pak, P. K. Patel, T. Parham, R. Petrasso, J. E. Ralph, H. Rinderknecht, S. P. Regan, H. F. Robey, J. S. Ross, J. D. Salmonson, C. Sangster, J. Sater, M. B. Schneider, F. H. Séguin, M. J. Shaw, M. J. Shoup, P. T. Springer, W. Stoeffl, L. J. Suter, C. A. Thomas, R. P. J. Town, C. Walters, S. V. Weber, P. J. Wegner, C. Widmayer, P. K. Whitman, K. Widmann, D. C. Wilson, B. M. Van Wonterghem, B. J. MacGowan, L. J. Atherton, and E. I. Moses, Plasma Phys. Control. Fusion **54**, 045013 (2012).

[3]O. L. Landen, O. L. Landen, R. Benedetti, D. Bleuel, T. R. Boehly, D. K. Bradley, J. A. Caggiano, D. A. Callahan, P. M. Celliers, C. J. Cerjan, D. Clark, G. W. Collins, E. L. Dewald, S. N. Dixit, T. Doeppner, D. Edgell, J. Eggert, D. Farley, J. A. Frenje, V. Glebov, S. M. Glenn, S. H. Glenzer, S. W. Haan, A. Hamza, B. A. Hammel, C. A. Haynam, J. H. Hammer, R. F. Heeter, H. W. Herrmann, D. G. Hicks, D. E. Hinkel, N. Izumi, M. Gatu Johnson, O. S. Jones, D. H. Kalantar, R. L. Kauffman, J. D. Kilkenny, J. L. Kline, J. P. Knauer, J. A. Koch, G. A. Kyrala, K. LaFortune, T. Ma, A. J. Mackinnon, A. J. Macphee, E. Mapoles, J. L. Milovich, J. D. Moody, N. B. Meezan, P. Michel, A. S. Moore, D. H. Munro, A. Nikroo, R. E. Olson, K. Opachich, A. Pak, T. Parham, P. Patel, H.-S. Park, R. P. Petrasso, J. Ralph, S. P. Regan, B. A. Remington, H. G. Rinderknecht, H. F. Robey, M. D. Rosen, J. S. Ross, J. D. Salmonson, T. C. Sangster, M. B. Schneider, V. Smalyuk, B. K. Spears, P. T. Springer, L. J. Suter, C. A. Thomas, R. P. J. Town, S. V. Weber, P. J. Wegner, D. C. Wilson, K. Widmann, C. Yeamans, A. Zylstra, M. J. Edwards, J. D. Lindl, L. J. Atherton, W. W. Hsing, B. J. MacGowan, B. M. VanWonterghem, and E. I. Moses, Plasma Phys. Control. Fusion **54**, 124026 (2012).

[4]S. H. Glenzer, S. H. Glenzer, B. J. MacGowan, N. B. Meezan, P. A. Adams, J. B. Alfonso, E. T. Alger, Z. Alherz, L. F. Alvarez, S. S. Alvarez, P. V. Amick, K. S. Andersson, S. D. Andrews, G. J. Antonini, P. A. Arnold, D. P. Atkinson, L. Auyang, S. G. Azevedo, B. N. M. Balaoing, J. A. Baltz, F. Barbosa, G. W. Bardsley, D. A. Barker, A. I. Barnes, A. Baron, R. G. Beeler, B. V. Beeman, L. R. Belk, J. C. Bell, P. M. Bell, R. L. Berger, M. A. Bergonia, L. J. Bernardez, L. V. Berzins, R. C. Bettenhausen, L. Bezerides, S. D. Bhandarkar, C. L. Bishop, E. J. Bond, D. R. Bopp, J. A. Borgman, J. R. Bower, G. A. Bowers, M. W. Bowers, D. T. Boyle, D. K. Bradley, J. L. Bragg, J. Braucht, D. L. Brinkerhoff, D. F. Browning, G. K. Brunton, S. C. Burkhart, S. R. Burns, K. E. Burns, B. Burr, L. M. Burrows, R. K. Butlin, N. J. Cahayag, D. A. Callahan, P. S. Cardinale, R. W. Carey, J. W. Carlson, A. D. Casey, C. Castro, J. R. Celeste, A. Y. Chakicherla, F. W. Chambers, C. Chan, H. Chandrasekaran, C. Chang, R. F. Chapman, K. Charron, Y. Chen, M. J. Christensen, A. J. Churby, T. J. Clancy, B. D. Cline, L. C. Clowdus, D. G. Cocherell, F. E. Coffield, S. J. Cohen, R. L. Costa, J. R. Cox, G. M. Curnow, M. J. Dailey, P. M. Danforth, R. Darbee, P. S. Datte, J. A. Davis, G. A. Deis, R. D. Demaret, E. L. Dewald, P. Di Nicola, J. M. Di Nicola, L. Divol, S. Dixit, D. B. Dobson, T. Doppner, J. D. Driscoll, J. Dugorepec, J. J. Duncan, P. C. Dupuy, E. G. Dzenitis, M. J. Eckart, S. L. Edson, G. J. Edwards, M. J. Edwards, O. D. Edwards, P. W. Edwards, J. C. Ellefson, C. H. Ellerbee, G. V. Erbert, C. M. Estes, W. J. Fabyan, R. N. Fallejo, M. Fedorov, B. Felker, J. T. Fink, M. D. Finney, L. F. Finnie, M. J. Fischer, J. M. Fisher, B. T. Fishler, J. W. Florio, A. Forsman, C. B. Foxworthy, R. M. Franks, T. Frazier, G. Frieder, T. Fung, G. N. Gawinski, C. R. Gibson, E. Giraldez, S. M. Glenn, B. P. Golick, H. Gonzales, S. A. Gonzales, M. J. Gonzalez, K. L. Griffin, J. Grippen, S. M. Gross, P. H. Gschweng, G. Gururangan, K. Gu, S. W. Haan, S. R. Hahn, B. J. Haid, J. E. Hamblen, B. A. Hammel, A. V. Hamza, D. L. Hardy, D. R. Hart, R. G. Hartley, C. A. Haynam, G. M. Heestand, M. R. Hermann, G. L. Hermes, D. S. Hey, R. L. Hibbard, D. G. Hicks, D. E. Hinkel, D. L. Hipple, J. D. Hitchcock, D. L. Hodtwalker, J. P. Holder, J. D. Hollis, G. M. Holtmeier, S. R. Huber, A. W. Huey, D. N. Hulsey, S. L. Hunter, T. R. Huppler, M. S. Hutton, N. Izumi, J. L. Jackson, M. A. Jackson, K. S. Jancaitis, D. R. Jedlovec, B. Johnson, M. C. Johnson, T. Johnson, M. P. Johnston, O. S. Jones, D. H. Kalantar, J. H. Kamperschroer, R. L. Kauffman, G. A. Keating, L. M. Kegelmeyer, S. L. Kenitzer, J. R. Kimbrough, K. King, R. K. Kirkwood, J. L. Klingmann, K. M. Knittel, T. R. Kohut, K. G. Koka, S. W. Kramer, J. E. Krammen, K. G. Krauter, G. W. Krauter, E. K. Krieger, J. J. Kroll, K. N. La Fortune, L. J. Lagin, V. K. Lakamsani, O. L. Landen, S. W. Lane, A. B. Langdon, S. H. Langer, N. Lao, D. W. Larson, D. Latray, G. T. Lau, S. Le Pape, B. L. Lechleiter, Y. Lee, T. L. Lee, J. Li, J. A. Liebman, J. D. Lindl, S. F. Locke, H. K. Loey, R. A. London, F. J. Lopez, D. M. Lord, R. R. Lowe-Webb, J. G. Lown, A. P. Ludwigsen, N. W. Lum, R. R. Lyons, T. Ma, A. J. MacKinnon, M. D. Magat, D. T. Maloy, T. N. Malsbury, G. Markham, R. M. Marquez, A. A. Marsh, C. D. Marshall, S. R. Marshall, I. L. Maslennikov, D. G. Mathisen, G. J. Mauger, M.-Y. Mauvais, J. A. McBride, T. McCarville, J. B. McCloud, A. McGrew, B. McHale, A. G. MacPhee, J. F. Meeker, J. S. Merill, E. P. Mertens, P. A. Michel, M. G. Miller, T. Mills, J. L. Milovich, R. Miramontes, R. C. Montesanti, M. M. Montoya, J. Moody, J. D. Moody, K. A. Moreno, J. Morris, K. M. Morriston, J. R. Nelson, M. Neto, J. D. Neumann, E. Ng, Q. M. Ngo, B. L. Olejniczak, R. E. Olson, N. L. Orsi, M. W. Owens, E. H. Padilla, T. M. Pannell, T. G. Parham, R. W. Patterson, Jr., G. Pavel, R. R. Prasad, D. Pendlton, F. A. Penko, B. L. Pepmeier, D. E. Petersen, T. W. Phillips, D. Pigg, K. W. Piston, K. D. Pletcher, C. L. Powell, H. B. Radousky, B. S. Raimondi, J. E. Ralph, R. L. Rampke, R. K. Reed, W. A. Reid, V. V. Rekow, J. L. Reynolds, J. J. Rhodes, M. J. Richardson, R. J. Rinnert, B. P. Riordan, A. S. Rivenes, A. T. Rivera, C. J. Roberts, J. A. Robinson, R. B. Robinson, S. R. Robison, O. R. Rodriguez, S. P. Rogers, M. D. Rosen, G. F. Ross, M. Runkel, A. S. Runtal, R. A. Sacks, S. F. Sailors, J. T. Salmon, J. D. Salmonson, R. L. Saunders, J. R. Schaffer, T. M. Schindler, M. J. Schmitt, M. B. Schneider, K. S. Segraves, M. J. Shaw, M. E. Sheldrick, R. T. Shelton, M. K. Shiflett, S. J. Shiromizu, M. Shor, L. L. Silva, S. A. Silva, K. M. Skulina, D. A. Smauley, B. E. Smith, L. K. Smith, A. L. Solomon, S. Sommer, J. G. Soto, N. I. Spafford, D. E. Speck, P. T. Springer, M. Stadermann, F. Stanley, T. G. Stone, E. A. Stout, P. L. Stratton, R. J. Strausser, L. J. Suter, W. Sweet, M. F. Swisher, J. D. Tappero, J. B. Tassano, J. S. Taylor, E. A. Tekle, C. Thai, C. A. Thomas, A. Thomas, A. L. Throop, G. L. Tietbohl, J. M. Tillman, R. P. J. Town, S. L. Townsend, K. L. Tribbey, D. Trummer, J. Truong, J. Vaher, M. Valadez, P. Van Arsdall, A. J. Van Prooyen, E. O. Vergel de Dios, M. D. Vergino1, S. P. Vernon, J. L. Vickers, G. T. Villanueva, M. A. Vitalich, S. A. Vonhof, F. E. Wade, R. J. Wallace, C. T. Warren, A. L. Warrick, J. Watkins, S. Weaver, P. J. Wegner, M. A. Weingart, J. Wen, K. S. White, P. K. Whitman, K. Widmann, C. C. Widmayer, K. Wilhelmsen, E. A. Williams, W. H. Williams, L. Willis, E. F. Wilson, B. A. Wilson, M. C. Witte, K. Work, P. S. Yang, B. K. Young, K. P. Youngblood, R. A. Zacharias, T. Zaleski, P. G. Zapata, H. Zhang, J. S. Zielinski, J. L. Kline, G. A. Kyrala, C. Niemann, J. D. Kilkenny, A. Nikroo, B. M. Van Wonterghem, L. J. Atherton, and E. I. Moses, Phys. Rev. Lett. **106**, 085004 (2011).

[5]N. B. Meezan, L. J. Atherton, D. A. Callahan, E. L. Dewald, S. Dixit, E. G. Dzenitis, M. J. Edwards, C. A. Haynam, D. E. Hinkel, O. S. Jones, O. Landen, R. A. London, P. A. Michel, J. D. Moody, J. L. Milovich, M. B. Schneider, C. A. Thomas, R. P. J. Town, A. L. Warrick, S. V. Weber, K. Widmann, S. H. Glenzer, L. J. Suter, B. J. MacGowan, J. L. Kline, G. A. Kyrala, and A. Nikroo, Phys. Plasmas **17**, 056304 (2010).

[6]S. W. Haan, J. D. Lindl, D. A. Callahan, D. S. Clark, J. D. Salmonson, B. A. Hammel, L. J. Atherton, R. C. Cook, M. J. Edwards, S. Glenzer, A. V. Hamza, S. P. Hatchett, M. C. Herrmann, D. E. Hinkel, D. D. Ho, H. Huang, O. S. Jones, J. Kline, G. Kyrala, O. L. Landen, B. J. MacGowan, M. M. Marinak, D. D. Meyerhofer, J. L. Milovich, K. A. Moreno, E. I. Moses, D. H. Munro, A. Nikroo, R. E. Olson, K. Peterson, S. M. Pollaine, J. E. Ralph, H. F. Robey, B. K. Spears, P. T. Springer, L. J. Suter, C. A. Thomas, R. P. Town, R. Vesey, S. V. Weber, H. L. Wilkens, and D. C. Wilson, Phys. Plasmas **18**, 051001 (2011).

[7]S. H. Glenzer, B. J. MacGowan, P. Michel, N. B. Meezan, L. J. Suter, S. N. Dixit, J. L. Kline, G. A. Kyrala, D. K. Bradley, D. A. Callahan, E. L. Dewald, L. Divol, E. Dzenitis, M. J. Edwards, A. V. Hamza, C. A. Haynam, D. E. Hinkel, D. H. Kalantar, J. D. Kilkenny, O. L. Landen, J. D. Lindl, S. LePape, J. D. Moody, A. Nikroo, T. Parham, M. B. Schneider, R. P. J. Town, P. Wegner, K. Widmann, P. Whitman, B. K. F. Young, B. Van Wonterghem, L. J. Atherton, and E. L. Moses, Science **327**, 1228 (2010).

[8]P. Michel, L. Divol, E. A. Williams, S. Weber, C. A. Thomas, D. A. Callahan, S. W. Haan, J. D. Salmonson, S. Dixit, D. E. Hinkel, M. J. Edwards, B. J. MacGowan, J. D. Lindl, S. H. Glenzer, and L. J. Suter, Phys. Rev. Lett. **102**, 025004 (2009).

[9]G. A. Kyrala, J. L. Kline, S. Dixit, S. Glenzer, D. Kalantar, D. Bradley, N. Izumi, N. Meezan, O. Landen, D. Callahan, S. V. Weber, J. P. Holder, S. Glenn, M. J. Edwards, J. Koch, L. J. Suter, S. W. Haan, R. P. J. Town, P. Michel, O. Jones, S. Langer, J. D. Moody, E. L. Dewald, T. Ma, J. Ralph, A. Hamza, E. Dzenitis, and J. Kilkenny, Phys. Plasmas **18**, 056307 (2011).

[10]R. P. J. Town, M. D. Rosen, P. A. Michel, L. Divol, J. D. Moody, G. A. Kyrala, M. B. Schneider, J. L. Kline, C. A. Thomas, J. L. Milovich, D. A. Callahan, N. B. Meezan, D. E. Hinkel, E. A. Williams, R. L. Berger, M. J. Edwards, L. J. Suter, S. W. Haan, J. D. Lindl, E. L. Dewald, S. Dixit, S. H. Glenzer, O. L. Landen, E. I. Moses, H. A. Scott, J. A. Harte, and G. B. Zimmerman, Phys. Plasmas **18**, 056302 (2011).

[11]M. D. Rosen, H. A. Scott, D. E. Hinkel, E. A. Williams, D. A. Callahan, R. P. J. Town, L. Divol, P. A. Michel, W. L. Kruer, L. J. Suter, R. A. London, J. A. Harte, and G. B. Zimmerman, High Energy Density Phys. **7**(3), 180 (2011).

[12]J. A. Frenje, R. Bionta, E. J. Bond, J. A. Caggiano, D. T. Casey, C. Cerjan, J. Edwards, M. Eckart, D. N. Fittinghoff, S. Friedrich, V. Yu. Glebov, S. Glenzer, G. Grim, S. Haan, R. Hatarik, S. Hatchett, M. Gatu Johnson, O. S. Jones, J. D. Kilkenny, J. P. Knauer, O. Landen, R. Leeper, S. Le Pape, R. Lerche, C. K. Li, A. Mackinnon, J. McNaney, F. E. Merrill, M. Moran, D. H. Munro, T. J. Murphy, R. D. Petrasso, R. Rygg, T. C. Sangster, F. H. Séguin, S. Sepke, B. Spears, P. Springer, C. Stoeckl, and D. C. Wilson, Nucl. Fusion **53**, 043014 (2013).

[13]T. Ma, P. K. Patel, N. Izumi, P. T. Springer, M. H. Key, L. J. Atherton, L. R. Benedetti, D. K. Bradley, D. A. Callahan, P. M. Celliers, C. J. Cerjan, D. S. Clark, E. L. Dewald, S. N. Dixit, T. Doppner, D. H. Edgell, R. Epstein, S. Glenn, G. Grim, S. W. Haan, B. A. Hammel, D. Hicks, W. W. Hsing, O. S. Jones, S. F. Khan, J. D. Kilkenny, J. L. Kline, G. A. Kyrala, O. L. Landen, S. Le Pape, B. J. MacGowan, A. J. Mackinnon, A. G. MacPhee, N. B. Meezan, J. D. Moody, A. Pak, T. Parham, H.-S. Park, J. E. Ralph, S. P. Regan, B. A. Remington, H. F. Robey, J. S. Ross, B. K. Spears, V. Smalyuk, L. J. Suter, R. Tommasini, R. P. Town, S. V. Weber, J. D. Lindl, M. J. Edwards, S. H. Glenzer, and E. I. Moses, "Onset of hydrodynamic mix in high-velocity, highly compressed inertial confinement fusion," Phys. Rev. Lett. (submitted).

[14]H. A. Scott and S. B. Hansen, High Energy Density Phys. **6**, 39 (2010).

[15]M. Gatu Johnson, J. A. Frenje, D. T. Casey, C. K. Li, F. H. Séguin, R. Petrasso, R. Ashabranner, R. M. Bionta, D. L. Bleuel, E. J. Bond, J. A. Caggiano, A. Carpenter, C. J. Cerjan, T. J. Clancy, T. Doeppner, M. J.

Eckart, M. J. Edwards, S. Friedrich, S. H. Glenzer, S. W. Haan, E. P. Hartouni, R. Hatarik, S. P. Hatchett, O. S. Jones, G. Kyrala, S. Le Pape, R. A. Lerche, O. L. Landen, T. Ma, A. J. MacKinnon, M. A. McKernan, M. J. Moran, E. Moses, D. H. Munro, J. McNaney, H. S. Park, J. Ralph, B. Remington, J. R. Rygg, S. M. Sepke, V. Smalyuk, B. Spears, P. T. Springer, C. B. Yeamans, M. Farrell, D. Jasion, J. D. Kilkenny, A. Nikroo, R. Paguio, J. P. Knauer, V. Yu Glebov, T. C. Sangster, R. Betti, C. Stoeckl, J. Magoon, M. J. Shoup III, G. P. Grim, J. Kline, G. L. Morgan, T. J. Murphy, R. J. Leeper, C. L. Ruiz, G. W. Cooper, and A. J. Nelson, Rev. Sci. Instrm. **83**, 10D308 (2012).

[16]D. Bleuel, C. B. Yeamans, L. A. Bernstein, R. M. Bionta, J. A. Caggiano, D. T. Casey, G. W. Cooper, O. B. Drury, J. A. Frenje, C. A. Hagmann, R. Hatarik, J. P. Knauer, M. Gatu Johnson, K. M. Knittel, R. J. Leeper, J. M. McNaney, M. Moran, C. L. Ruiz, and D. H. G. Schneider, Rev. Sci. Instrm. **83**, 10D313 (2012).

[17]V. Yu. Glebov, T. C. Sangster, C. Stoeckl, J. P. Knauer, W. Theobald, K. L. Marshall, M. J. Shoup III, T. Buczek, M. Cruz, T. Duffy, M. Romanofsky, M. Fox, A. Pruyne, M. J. Moran, R. A. Lerche, J. McNaney, J. D. Kilkenny, M. J. Eckart, D. Schneider, D. Munro, W. Stoeffl, R. Zacharias, J. J. Haslam, T. Clancy, M. Yeoman, D. Warwas, C. J. Horsfield, J.-L. Bourgade, O. Landoas, L. Disdier, G. A. Chandler, and R. J. Leeper, Rev. Sci. Instrm. **81**, 10D325 (2010).

[18]T. Ma, N. Izumi, R. Tommasini, D. K. Bradley, P. Bell, C. J. Cerjan, S. Dixit, T. Doppner, O. Jones, J. L. Kline, G. Kyrala, O. L. Landen, S. Le Pape, A. J. Mackinnon, H.-S. Park, P. K. Patel, R. R. Prasad, J. Ralph, S. P. Regan, V. A. Smalyuk, P. T. Springer, L. Suter, R. P. J. Town, S. V. Weber, and S. H. Glenzer, Rev. Sci. Instrm. **83**, 10E115 (2012).

[19]N. Izumi, T. Ma, M. Barrios, L. R. Benedetti, D. Callahan, C. Cerjan, J. Edwards, S. Glenn, S. Glenzer, J. Kilkenny, J. Kline, G. Kyrala, O. L. Landen, S. Regan, P. T. Springer, L. Suter, R. Tommasini, R. Town, A. J. Mackinnon, P. Bell, and D. K. Bradley, Rev. Sci. Instrm. **83**, 10E121 (2012).

[20]A. G. MacPhee, D. H. Edgell, E. J. Bond, D. K. Bradley, C. G. Brown, S. R. Burns, J. R. Celeste, C. J. Cerjan, M. J. Eckart, V. Y. Glebov, S. H. Glenzer, D. S. Hey, O. S. Jones, J. D. Kilkenny, J. R. Kimbrough, O. L. Landen, A. J. Mackinnon, N. B. Meezan, J. M. Parker, and R. M. Sweeny, J. Instrumentation **6**, P02009 (2011).

[21]D. H. Edgell, D. K. Bradley, E. J. Bond, S. Burns, D. A. Callahan, J. Celeste, M. J. Eckart, V. Yu. Glebov, D. S. Hey, G. Lacaille, J. D. Kilkenny, J. Kimbrough, A. J. Mackinnon, J. Magoon, J. Parker, T. C. Sangster, M. J. Shoup III, C. Stoeckl, T. Thomas, and A. G. MacPhee, Rev. Sci. Instr. **83**, 10E119 (2012).

[22]R. Betti, P. Y. Chang, B. K. Spears, K. S. Anderson, J. Edwards, M. Fatenejad, J. D. Lindl, R. L. McCrory, R. Nora, and D. Shvarts, Phys. Plasmas **17**, 058102 (2010).

[23]D. S. Clark, D. E. Hinkel, D. C. Eder, O. S. Jones, S. W. Haan, B. A. Hammel, M. M. Marinak, J. L. Milovich, H. F. Robey, L. J. Suter, and R. P. J. Town, Phys. Plasmas **20**, 056318 (2013).

[24]H. R. Robey, P. M. Celliers, J. L. Kline, A. J. Mackinnon, T. R. Boehly, O. L. Landen, J. H. Eggert, D. Hicks, S. Le Pape, D. R. Farley, M. W. Bowers, K. G. Krauter, D. H. Munro, O. S. Jones, J. L. Milovich, D. Clark, B. K. Spears, R. P. J. Town, S. W. Haan, S. Dixit, M. B. Schneider, E. L. Dewald, K. Widmann, J. D. Moody, T. D. Döppner, H. B. Radousky, A. Nikroo, J. J. Kroll, A. V. Hamza, J. B. Horner, S. D. Bhandarkar, E. Dzenitis, E. Alger, E. Giraldez, C. Castro, K. Moreno, C. Haynam, K. N. LaFortune, C. Widmayer, M. Shaw, K. Jancaitis, T. Parham, D. M. Holunga, C. F. Walters, B. Haid, T. Malsbury, D. Trummer, K. R. Coffee, B. Burr, L. V. Berzins, C. Choate, S. J. Brereton, S. Azevedo, H. Chandrasekaran, S. Glenzer, J. A. Caggiano, J. P. Knauer, J. A. Frenje, D. T. Casey, M. Gatu Johnson, F. H. Séguin, B. K. Young, M. J. Edwards, B. M. Van Wonterghem, J. Kilkenny, B. J. MacGowan, J. Atherton, J. D. Lindl, D. D. Meyerhofer, and E. Moses, Phys. Rev. Lett. **108**, 215004 (2012).

[25]D. G. Hicks, N. B. Meezan, E. L. Dewald, A. J. Mackinnon, R. E. Olson, D. A. Callahan, T. Döppner, L. R. Benedetti, D. K. Bradley, P. M. Celliers, D. S. Clark, P. Di Nicola, S. N. Dixit, E. G. Dzenitis, J. E. Eggert, D. R. Farley, J. A. Frenje, S. M. Glenn, S. H. Glenzer, A. V. Hamza, R. F. Heeter, J. P. Holder, N. Izumi, D. H. Kalantar, S. F. Khan, J. L. Kline, J. J. Kroll, G. A. Kyrala, T. Ma, A. G. MacPhee, J. M. McNaney, J. D. Moody, M. J. Moran, B. R. Nathan, A. Nikroo, Y. P. Opachich, R. D. Petrasso, R. R. Prasad, J. E. Ralph, H. F. Robey, H. G. Rinderknecht, J. R. Rygg, J. D. Salmonson, M. B. Schneider, N. Simanovskaia, B. K. Spears, R. Tommasini, K. Widmann, A. B. Zylstra, G. W. Collins, O. L. Landen, J. D. Kilkenny, W. W. Hsing, B. J. MacGowan, L. J. Atherton, and M. J. Edwards, Phys. Plasmas **19**, 122702 (2012).

[26]N. B. Meezan, A. J. MacKinnon, D. G. Hicks, E. L. Dewald, R. Tommasini, S. Le Pape, T. Doppner, T. Ma, D. R. Farley, D. H. Kalantar, P. Di Nicola, D. A. Callahan, H. F. Robey, C. A. Thomas, S. T. Prisbrey, O. S. Jones, J. L. Milovich, D. S. Clark, D. C. Eder, M. B. Schneider, K. Widmann, J. A. Koch, J. D. Salmonson, Y. P. Opachich, L. R. Benedetti, S. F. Khan, A. G. MacPhee, S. M. Glenn, D. K. Bradley, E. G. Dzenitis, B. R. Nathan, J. J. Kroll, A. V. Hamza, S. N. Dixit, L. J. Atherton, O. L. Landen, S. H. Glenzer, W. W. Hsing, L. J. Suter, M. J. Edwards, B. J. MacGowan, and E. I. Moses, Phys. Plasmas **20**, 056311 (2013).

[27]H. W. Hermann, N. Hoffman, D. C. Wilson, W. Stoeffl, L. Dauffy, Y. H. Kim, A. McEvoy, C. S. Young, J. M. Mack, C. J. Horsfield, M. Rubery, E. K. Miller, and Z. A. Ali, Rev. Sci. Instrm. **81**, 10D333 (2010).

[28]O. S. Jones, C. J. Cerjan, M. M. Marinak, J. L. Milovich, H. F. Robey, P. T. Springer, L. R. Benedetti, D. L. Bleuel, E. J. Bond, D. K. Bradley, D. A. Callahan, J. A. Caggiano, P. M. Celliers, D. S. Clark, S. M. Dixit, T. Doppner, R. J. Dylla-Spears, E. G. Dzentitis, D. R. Farley, S. M. Glenn, S. H. Glenzer, S. W. Haan, B. J. Haid, C. A. Haynam, D. G. Hicks, B. J. Kozioziemski, K. N. LaFortune, O. L. Landen, E. R. Mapoles, A. J. Mackinnon, J. M. McNaney, N. B. Meezan, P. A. Michel, J. D. Moody, M. J. Moran, D. H. Munro, M. V. Patel, T. G. Parham, J. D. Sater, S. M. Sepke, B. K. Spears, R. P. J. Town, S. V. Weber, K. Widmann, C. C. Widmayer, E. A. Williams, L. J. Atherton, M. J. Edwards, J. D. Lindl, B. J. MacGowan, L. J. Suter, R. E. Olson, H. W. Herrmann, J. L. Kline, G. A. Kyrala, D. C. Wilson, J. Frenje, T. R. Boehly, V. Glebov, J. P. Knauer, A. Nikroo, H. Wilkens, and J. D. Kilkenny, Phys. Plasmas **19**, 056315 (2012).

[29]C. Cerjan, P. T. Springer, and S. M. Sepke, Phys. Plasmas **20**, 056319 (2013).